J. Plasma Phys. (2017), *vol.* 83, 905830301
doi:10.1017/S0022377817000319

The development of magnetic field line wander in gyrokinetic plasma turbulence: dependence on amplitude of turbulence

Sofiane Bourouaine[1,2,†] **and Gregory G. Howes**[1]

[1]Department of Physics and Astronomy, University of Iowa, Iowa City IA 54224, USA

[2]Physics and Space Sciences, Florida Institute of Technology, 150 w University blvd, Melbourne, FL 32904, USA

(Received 2 December 2016; revised 2 April 2017; accepted 4 April 2017)

The dynamics of a turbulent plasma not only manifests the transport of energy from large to small scales, but also can lead to a tangling of the magnetic field that threads through the plasma. The resulting magnetic field line wander can have a large impact on a number of other important processes, such as the propagation of energetic particles through the turbulent plasma. Here we explore the saturation of the turbulent cascade, the development of stochasticity due to turbulent tangling of the magnetic field lines and the separation of field lines through the turbulent dynamics using nonlinear gyrokinetic simulations of weakly collisional plasma turbulence, relevant to many turbulent space and astrophysical plasma environments. We determine the characteristic time t_2 for the saturation of the turbulent perpendicular magnetic energy spectrum. We find that the turbulent magnetic field becomes completely stochastic at time $t \lesssim t_2$ for strong turbulence, and at $t \gtrsim t_2$ for weak turbulence. However, when the nonlinearity parameter of the turbulence, a dimensionless measure of the amplitude of the turbulence, reaches a threshold value (within the regime of weak turbulence) the magnetic field stochasticity does not fully develop, at least within the evolution time interval $t_2 < t \leqslant 13t_2$. Finally, we quantify the mean square displacement of magnetic field lines in the turbulent magnetic field with a functional form $\langle(\delta r)^2\rangle = A(z/L_\parallel)^p$ ($L_\parallel$ is the correlation length parallel to the magnetic background field $\boldsymbol{B_0}$, z is the distance along $\boldsymbol{B_0}$ direction), providing functional forms of the amplitude coefficient A and power-law exponent p as a function of the nonlinearity parameter.

Key words: plasma nonlinear phenomena, plasma waves, space plasma physics

1. Introduction

Turbulence in space and terrestrial laboratory plasmas remains one of the most active research areas in plasma physics. Space and fusion plasmas are turbulent, weakly collisional and magnetized. Plasma turbulence governs particle and energy transport and describing such transport is a key goal of the plasma physics community. Turbulence in space plasmas likely plays an important role in several observed phenomena, such as solar coronal heating, solar wind heating and the acceleration of solar particles in the heliosphere. Furthermore, the turbulence also affects how solar

† Email address for correspondence: sbourouaine@fit.edu

energetic particles and cosmic rays propagate through space. In terrestrial laboratories, turbulence may reduce the confinement for plasma fusion by enhancing transport across the confining magnetic field.

Iroshnikov (1963) and Kraichnan (1965) independently developed an isotropic theory for incompressible magnetohydrodynamics (MHD) turbulence suggesting that the nonlinear interactions of the large-scale Alfvén waves lead to a turbulent energy cascade down to smaller scales. Years after, it was demonstrated that anisotropy is an important characteristic in incompressible MHD turbulence, i.e. the anisotropic turbulent cascade transfers energy to smaller scales in the perpendicular direction with respect to the background magnetic field (Sridhar & Goldreich 1994; Goldreich & Sridhar 1995; Montgomery & Matthaeus 1995; Ghosh & Goldstein 1997; Matthaeus *et al.* 1998; Cho & Vishniac 2000; Maron & Goldreich 2001). The phenomenon of turbulent cascade due to the nonlinear interactions between counterpropagating Alfvén waves, which is the fundamental building block of plasma turbulence, has been experimentally tested (Howes *et al.* 2012; Drake *et al.* 2013; Howes & Nielson 2013; Howes *et al.* 2013; Nielson, Howes & Dorland 2013).

One significant effect of the turbulence is the tangling of the magnetic field lines, or magnetic field wander. Due to plasma turbulence, the magnetic field lines may become stochastic and get separated from each other leading to the spreading of particles that travel along the field lines. The magnetic field wander in turbulent plasmas impacts the propagation of the energetic particles in astrophysical space as well as the heat and particle transport in fusion plasmas. The problem of field line wandering and its impacts on other physical processes is one of the unresolved problems of plasma physics. For instance, understanding the wandering of magnetic field lines in solar wind turbulence will enable the prediction of the scattering of the solar energetic particles – arising from coronal mass ejections and flares that may occur on the Sun's surface – determining the energetic particle fluxes near the Earth, where they can potentially damage communication satellites or harm astronauts in orbit.

Models of the propagation of the cosmic rays and the solar energetic particles through a stochastic magnetic field were first proposed by Jokipii (1966) and Jokipii & Parker (1968). The authors describe the transport of the energetic particles in the context of the field line random walk (FLRW) theory using a quasilinear statistical calculation of the motion of charged particles in a spatially random magnetic field. Advanced models implementing nonlinear calculations of FLRW theory were developed later to estimate the diffusion of the field line wandering (Matthaeus *et al.* 1995). Recently, several models were developed to study the separation of the magnetic field lines, implementing various models of turbulence, including slab turbulence (Schlickeiser 1989; Shalchi & Kourakis 2007*a*,*b*; Shalchi 2010*b*), two-dimensional turbulence (Shalchi & Kourakis 2007*a*,*b*; Guest & Shalchi 2012), composite models including slab plus two-dimensional components (Bieber, Wanner & Matthaeus 1996; Shalchi & Kourakis 2007*a*,*b*; Qin & Shalchi 2013) and other three-dimensional models including MHD turbulence (Zimbardo *et al.* 1995; Zimbardo, Veltri & Pommois 2000; Maron, Chandran & Blackman 2004; Zimbardo, Pommois & Veltri 2006; Shalchi 2010*a*; Ragot 2011; Beresnyak 2013; Ruffolo & Matthaeus 2013; Shalchi & Kolly 2013). In the latter works, the superdiffusive behaviour of the magnetic field lines has been confirmed in three-dimensional MHD simulations for scales comparable to or less than the injection scale l_0, but for scales much larger than l_0 the field lines follow a diffusive law.

The magnetic field line wander may also impact the process of magnetic reconnection. For instance, it has been shown that the rate of magnetic reconnection

https://doi.org/10.1017/S0022377817000319 Published online by Cambridge University Press

can be enhanced due to magnetic field line wandering (see e.g. Lazarian & Vishniac 1999; Lazarian, Vishniac & Cho 2004).

In fusion plasmas, it has been suggested that the destruction of the magnetic flux surfaces in a tokamak can be caused by magnetic field wander arising due to the turbulent fluctuations in the confining magnetic field (Rechester & Rosenbluth 1978). Many subsequent works investigated the role of the magnetic field line wander in enhancing heat transport in fusion plasmas (Krommes, Oberman & Kleva 1983; Haas & Thyagaraja 1986; Laval 1993; Spatschek 2008). Advanced direct numerical simulations of weakly collisional plasma turbulence using nonlinear gyrokinetic simulations were used to explore the role of the wandering of the magnetic field lines in fusion plasmas (Nevins, Wang & Candy 2011; Wang *et al.* 2011; Hatch *et al.* 2012, 2013). For example, it is found that the wandering of the magnetic field lines does occur in fusion plasmas, but that it does not significantly enhance the heat transport in the plasma (Nevins *et al.* 2011; Wang *et al.* 2011). Additionally, it has been shown that the stochasticity of the magnetic field lines in gyrokinetic turbulence may induce the non-zonal transition – proposed as an explanation of the high-β runaway – in CYCLONE base case plasmas once a certain threshold of electron normalized plasma pressure is exceeded (Pueschel, Terry & Hatch 2014).

Previous studies of magnetic field wander estimated what is called the mean square displacement, $\langle(\delta r)^2\rangle$, to describe the spread of the stochastic magnetic field lines. It is found that the quantity $\langle(\delta r)^2\rangle$ is fit to a power-law function, $\propto l_B^p$, (l_B is the distance along the magnetic field line), however, the value of p was found to vary from a model to another. For example, analytic modelling of anisotropic three-dimensional turbulence (Shalchi & Kolly 2013) shows that the wandering of the magnetic field lines is diffusive, i.e. $p=1$. Non-diffusive transport ($p\neq 1$) of the field line wandering has also been found in other analytical as well as numerical works (see e.g. Lazarian & Vishniac 1999; Shalchi & Kourakis 2007*a*,*b*; Beresnyak 2013; Lazarian & Yan 2014).

In this present work, we focus on the development of magnetic field wander using nonlinear gyrokinetic simulations of weakly collisional plasma turbulence. We will study how small-scale turbulence (turbulent fluctuations having scales ranging between ion and electron scales) affects the stochasticity and the separation of the magnetic field lines. In figure 1 we sketch the magnetic power spectrum of solar wind turbulence (Sahraoui *et al.* 2009; Alexandrova *et al.* 2012). The cascade of the energy starts to occur near the outer scale $l\approx 10^6$ km down to the electron scale. The gyrokinetic simulation considered in our study describes turbulence between ion and electron scales (see red box in figure 1). Within these scales it has been shown that the turbulent energy cascade is controlled by kinetic Alfvén wave turbulence (Howes *et al.* 2006). It is worth noting that a steeper magnetic power spectrum $\sim k^{-7/3}$ below the proton gyroscale was first obtained within electron MHD turbulence (see, e.g. Biskamp, Schwarz & Drake 1996; Biskamp *et al.* 1999; Cho & Lazarian 2004). As a consequence of applying critical balance conditions at subproton scales the anisotropy $k_\parallel \sim k_\perp^{1/3}$ ($k_\parallel$ and $k_\perp$ are the parallel and perpendicular wavenumber components with respect to the local magnetic field) was obtained in electron MHD turbulence (Cho & Lazarian 2004, 2009). Furthermore, Cho & Vishniac (2000) argued that this scale-dependent anisotropy can be measured only with respect to the local magnetic field direction rather than the global mean field.

We investigate two features that characterize the wandering of the magnetic field lines as a function of the amplitude of the turbulence: (i) the stochasticity of the field lines and (ii) the spreading of the magnetic field lines. Developing a simple

https://doi.org/10.1017/S0022377817000319 Published online by Cambridge University Press

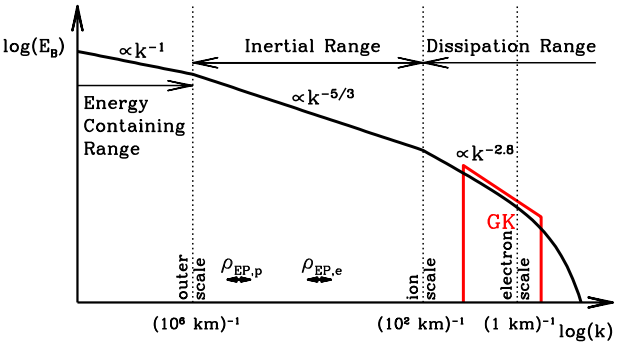

FIGURE 1. Schematic of the magnetic energy wavenumber spectrum in the solar wind showing the form of the spectrum in the energy containing inertial and dissipation ranges. Ranges for the typical Larmor radius scales for protons $\rho EP_{,p}$ and electrons $\rho EP_{,e}$ from solar energetic particle events are depicted. The area of the spectrum indicated by red line is the range of gyrokinetic (GK) turbulence scale considered in this study.

model of the spreading of magnetic field lines as a function of the amplitude of the turbulence is a critical step in constructing a reliable predictive model for the propagation of solar energetic particles in the heliosphere. The amplitude of the turbulence is characterized in our study by computing the nonlinearity parameter χ, a dimensionless measure of the ratio of the magnitude of the nonlinear to the linear terms in the equations of motion. Alternatively, the nonlinear parameter may be interpreted as $\chi \simeq t_l/t_n$, the ratio of the linear wave period t_l to the nonlinear time scale t_n. A unique aspect of this study is the use of nonlinear gyrokinetic simulations of turbulence – in which the microphysics of collisionless turbulent cascade and small-scale magnetic reconnection near the electron scales is resolved – to quantify the separation of the stochastic magnetic field lines.

2. Simulations and results

We use the astrophysical gyrokinetics code `AstroGK` to study the magnetic field line wander in gyrokinetic turbulence. The `AstroGK` code, which is described in detail in Numata *et al.* (2010), solves the gyrokinetic equation coupled to the gyro-averaged Maxwell equations (Frieman & Chen 1982; Howes *et al.* 2006). `AstroGK` computes the time evolution of the perturbed gyro-averaged distribution function h_s for each species s and the fluctuating electromagnetic fields, defined by the scalar potential ϕ, parallel vector potential $A_\parallel$ and the parallel magnetic field perturbation $\delta B_\parallel$. Here, $\parallel$ refers to the parallel direction with respect to the background magnetic field $\boldsymbol{B_0} = B_0\hat{\boldsymbol{z}}$. The simulation domain is assumed to be a periodic box elongated along the equilibrium magnetic field with size $L_\parallel \times L_\perp^2$, where $L_\perp$ ($L_\parallel$) is the size of the simulation box along x and y (along z direction) directions perpendicular to $\boldsymbol{B_0}$, and $L_\perp \ll L_\parallel$. We assume two plasma species, protons and electrons with a real mass ratio $m_i/m_e = 1836$.

The numerical code `AstroGK` has been used in early studies to investigate solar wind turbulence (Howes *et al.* 2008*b*, 2011*b*). Nonlinear gyrokinetic simulations (TenBarge & Howes 2013; TenBarge, Howes & Dorland 2013) have been found to reproduce the scaling of the turbulence magnetic energy spectrum waves down to the scales of the electron Larmor radius ρ_e, (Alexandrova *et al.* 2012). For our

https://doi.org/10.1017/S0022377817000319 Published online by Cambridge University Press

Simulation	$\overline{\chi} \pm \delta\chi$	t_1/t_l	t_2/t_l	t_f/t_l
Run 1	4.9 ± 0.8	0.064	0.27	1.1
Run 2	3.4 ± 0.6	0.10	0.21	2.2
Run 3	1.6 ± 0.2	0.15	0.29	3.6
Run 4	1.3 ± 0.2	0.3	0.40	4.7
Run 5	0.83 ± 0.06	0.28	1.3	8.2
Run 6	0.44 ± 0.05	0.28	1.4	15
Run 7	0.14 ± 0.01	0.31	2.2	29

TABLE 1. For simulation Runs 1–7, time-averaged nonlinearity parameter $\overline{\chi}$ with its standard deviation $\delta\chi$. Interaction time t_1, saturation time t_2 and final simulation time t_f normalized to the linear kinetic Alfvén wave period $t_l = 1.74\omega_{A0}^{-1}$ for the domain-scale waves at $k_\perp\rho_i = 5$.

study, we choose fixed plasma parameters for the proton-to-electron temperature ratio $T_i/T_e = 1$ and the proton plasma $\beta_i = 1$, where $\beta_i = v_{th_i}^2/v_A^2$, $v_{th_i} = (2T_i/m_i)^{1/2}$ is the ion thermal speed and v_A is the Alfvén speed. The spatial resolution of the simulation domain is $n_x \times n_y \times n_z = 64 \times 64 \times 32$, representing the number of points along x, y and z directions, and velocity space resolution is a polar grid of 32 pitch angles by 16 energy levels. Also, we choose $\epsilon = L_\perp/L_\parallel = 0.0163$. We use an oscillating Langevin antenna (TenBarge, Howes, Dorland & Hammett 2014) to drive four counterpropagating wave modes at the domain perpendicular scale $k_\perp\rho_i = 5$, where $k_\perp$ is the perpendicular wavenumber component and ρ_i is the proton Larmor radius. To investigate how the tangling of the magnetic field lines is affected by the amplitude of the turbulence we consider seven simulation runs differing only by the amplitude of the driving. The average value of the nonlinearity parameter for each of these runs is presented in table 1.

The specific definition used for the nonlinearity parameter in this paper is

$$\chi = b\frac{k_\perp \delta B_\perp(k_\perp)}{k_\parallel B_0}, \tag{2.1}$$

where b is an order-unity dimensionless parameter, B_0 is the equilibrium magnetic field amplitude, $\delta B_\perp(k_\perp)$ is the amplitude of fluctuations at a particular perpendicular Fourier wavenumber, $k_\perp = \sqrt{k_x^2 + k_y^2}$ and $k_\parallel$ is the average parallel wavenumber associated with magnetic field fluctuations having that particular perpendicular wavenumber. The strength of the nonlinearity in kinetic Alfvén wave turbulence is characterized by the nonlinearity parameter χ given in (2.1) and it is estimated in analogy to the one considered in incompressible MHD, i.e. the ratio of the magnitude of the nonlinear to the linear terms, $\chi \sim (k_\perp \delta v_\perp)/(k_\parallel v_{ph})$, where $\delta v_\perp$ is the fluctuating bulk velocity and v_{ph} is the phase speed of kinetic Alfvén waves (or Alfvén waves in case of incompressible MHD). First, we choose a value $b = 1$ for the order-unity parameter in our calculation of χ. Because the oscillating Langevin antenna (TenBarge *et al.* 2014) yields a finite-time correlated driving, the power input into the plasma varies with time, meaning that the amplitude of the turbulence, which determines the nonlinearity parameter, varies in time. Therefore, we specify here how to determine the nonlinearity parameter based on turbulent magnetic field at a single point in time. To avoid any direct influence of the driving at

https://doi.org/10.1017/S0022377817000319 Published online by Cambridge University Press

$k_\perp \rho_i = 5$ in our computation of the nonlinearity parameter for each run, we compute the nonlinearity parameter using the average amplitude of the seven perpendicular Fourier modes with $k_\perp \rho_i = 10$ and $k_\perp \rho_i = 25/\sqrt{5}$ to obtain a value $\delta B_\perp(k_\perp)$ at a mode-weighted average $\langle k_\perp \rho_i \rangle \simeq 10.67$. Here, three modes correspond to $k_\perp \rho_i = 10$ and four modes correspond to $k_\perp \rho_i = 25/\sqrt{5}$. We also estimate the weighted-average value of $\delta B_\perp$ in the expression (2.1) as $(3\delta B_\perp(k_\perp = 10) + 4\delta B_\perp(k_\perp = 25/\sqrt{5}))/7$. It is widely acknowledged that the turbulent cascade in magnetized plasma turbulence is anisotropic (Zweben, Menyuk & Taylor 1979; Montgomery & Turner 1981; Shebalin, Matthaeus & Montgomery 1983; Oughton, Priest & Matthaeus 1994; Sridhar & Goldreich 1994; Goldreich & Sridhar 1995; Cho & Vishniac 2000; Galtier *et al.* 2000; Boldyrev 2006), with energy transferred to smaller perpendicular scales more rapidly than to smaller parallel scales, leading to fluctuations with the characteristic anisotropy $k_\perp \gg k_\parallel$ at small scales. The estimation of the wavenumber parallel to the local total magnetic field (as opposed to the equilibrium magnetic field) is numerically challenging (TenBarge & Howes 2012), so we use the scaling expected for a kinetic Alfvén wave cascade $k_\parallel \propto k_\perp^{1/3}$, giving a value $k_\parallel(k_\perp \rho_i = 10.67) \simeq 1.29 k_{\parallel 0}$ with $k_{\parallel 0} = 2\pi/L_\parallel$. With these specific choices, the nonlinearity parameter for each simulation can be computed as a function of time, $\chi(t)$. Table 1 lists the average value of the nonlinearity parameter $\overline{\chi}$ and its standard deviation $\delta\chi$ for Runs 1–7, taken over the period over which each simulation is saturated, $t_2 < t < t_f$, as discussed in § 2.1.

The characteristic linear time scale t_l is estimated from the linear frequency of a kinetic Alfvén wave at the domain scale, $k_\perp \rho_i = 5$. A numerical solution of the collisionless linear gyrokinetic dispersion relation (Howes *et al.* 2006) for the kinetic Alfvén wave frequency of these domain-scale waves gives $\omega_0 = 3.6\omega_{A0}$ where $\omega_{A0} = k_{\parallel 0} V_A$, or a linear kinetic Alfvén wave period $t_l = 1.74\omega_{A0}^{-1}$.

The turbulence is initially driven by four counterpropagating kinetic Alfvén wave modes with $(k_{\perp 0}\rho_i, k_{\perp 0}\rho_i, k_{\parallel 0}\rho_i/\epsilon) = (5, 0, \pm 1)$ and $(0, 5, \pm 1)$, where $k_{\perp 0} = 2\pi/L_\perp$ and $\epsilon = \rho_i/(2\pi L_\parallel)$.

Coulomb collisions in the gyrokinetic simulations are included (Abel *et al.* 2008; Barnes *et al.* 2009) to smooth out the small-scale structures that develop in velocity space, enabling irreversibility of the plasma heating process (Howes *et al.* 2006). We specify ion and electron collision frequencies $\nu_i = 0.2\omega_{A0}$ and $\nu_e = 0.5\omega_{A0}$, leading to weakly collisional dynamics with $\nu_s/\omega_0 \ll 1$. The numerical convergence of the power spectrum was already tested for simulation run 3 by doubling the spatial resolution of the simulation and verifying that the saturated magnetic energy spectrum was unchanged, and it is reported in TenBarge & Howes (2013) (see figure 1).

2.1. *Development and saturation of the turbulent magnetic power spectrum*

As modes driven at the scale of the simulation domain rise in amplitude, they begin to interact nonlinearly, leading to a cascade of their energy to smaller scales. After sufficient time has passed, the turbulent energy dissipated by kinetic mechanisms rises to match the energy input into the turbulence by the driving, causing the turbulent energy spectrum to reach a statistically steady state. In figure 2, we display the one-dimensional perpendicular magnetic power spectrum, $E_\perp(k_\perp) = \int \mathrm{d}k_z \int \mathrm{d}\theta k_\perp |\delta \boldsymbol{B}_\perp(\boldsymbol{k})|^2/8\pi$, where the wavevector components are expressed in cylindrical coordinates $(k_\perp, \theta, k_z)$. The spectra shown in figure 2 range from over-strong turbulence with $\chi > 1$ (Run 1, blue), critically balanced, strong turbulence with $\chi \simeq 1$ (Run 4, red) to weak turbulence with $\chi < 1$ (Run 6, yellow). The $E_\perp(k_\perp)$

https://doi.org/10.1017/S0022377817000319 Published online by Cambridge University Press

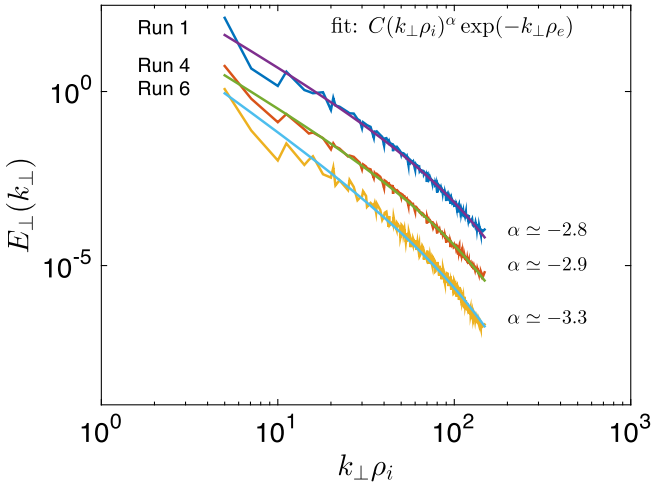

FIGURE 2. The time-averaged one-dimensional perpendicular magnetic energy spectrum $E_\perp(k_\perp)$ computed for three kinetic Alfvén wave turbulence simulations: Run 1 (blue) with $\overline{\chi} = 4.9$, Run 4 (red) with $\overline{\chi} = 1.3$ and Run 6 (yellow) with $\overline{\chi} = 0.44$. Fits to $C(k_\perp\rho_i)^\alpha \exp(-k_\perp\rho_e)$ are overplotted.

spectra plotted here are obtained through averaging over the full time interval from the saturation of the turbulent cascade (at time t_2, as defined below) until the end of the simulation at t_f. These time averaged $E_\perp(k_\perp)$ spectra are fit to the function $C(k_\perp\rho_i)^\alpha \exp(-k_\perp\rho_e)$ (Alexandrova *et al.* 2012; TenBarge *et al.* 2013), where C and α are fitting parameters and $\rho_e = v_{th_e}/\Omega_e$ is the electron Larmor gyroradius.

We evaluate the time scale of the saturation of the turbulent magnetic energy spectrum by following the evolution of the amplitude of the spectrum at $k_\perp\rho_i = 20.6$, a position in the middle of the dynamic range of the simulation, as a function of the normalized time t/t_l. Figure 3(*a*) displays the time evolution of the one-dimensional perpendicular magnetic spectrum $E_\perp(k_\perp\rho_i = 20.6)$ for Run 1 ($\overline{\chi} = 4.9$), Run 2 ($\overline{\chi} = 3.4$) and Run 3 ($\overline{\chi} = 1.6$), left to right. These runs correspond to a range of turbulent amplitudes, from over-strong turbulence (above critical balance) with $\chi > 1$ to approximately critically balanced, strong turbulence with $\chi \simeq 1$. These plots demonstrate the existence of two time scales that characterize the evolution of the turbulent magnetic field when driving by counterpropagating kinetic Alfvén waves from uniform magnetic field conditions. First, the energy in Fourier modes with $k_\perp\rho_i = 20.6$ rises as a steep power law in time $\propto t^{b_1}$ for times $t < t_1$, denoted by the first vertical blue line in figure 3. Next, the rate of increase of energy in mode $k_\perp\rho_i = 20.6$ decreases to less steep approximate power law $\propto t^{b_2}$, with $b_2 < b_1$, over the time interval $t_1 < t < t_2$. For times $t > t_2$, the energy in modes with $k_\perp\rho_i = 20.6$ remains approximately constant, indicating that the region of the turbulent cascade has reached a statistically steady state.

We interpret these two time scales in the following way. At times $t < t_1$, the energy of the modes with $k_\perp\rho_i = 20.6$ is dominated by the energy input from nonlinear interactions among lower wavenumber modes, leading to simple power-law increase in amplitude. At $t = t_1$, the amplitude of the modes with $k_\perp\rho_i = 20.6$ has risen to a sufficient level that these modes are able to interact nonlinearly with counterpropagating fluctuations to transfer their energy to yet higher wavenumber

https://doi.org/10.1017/S0022377817000319 Published online by Cambridge University Press

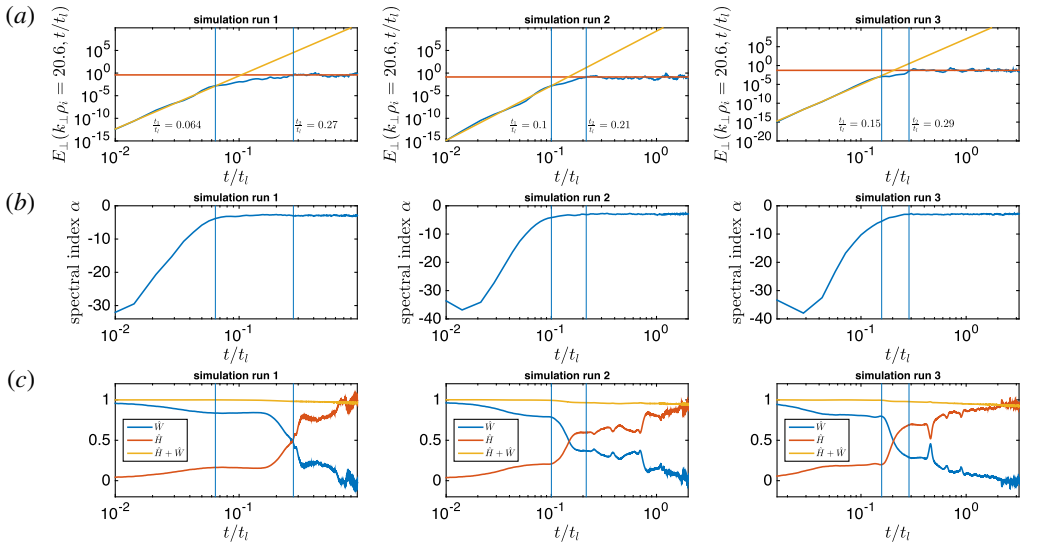

FIGURE 3. The time evolution of (*a*) the perpendicular magnetic energy spectrum $E_\perp(k_\perp\rho_i = 20.6)$, (*b*) the spectral index α from the fit to the function $A(k_\perp\rho_i)^\alpha \exp(-k_\perp\rho_e)$, (*c*) the normalized total heating rate, $\hat{H} = H/P_{in}$, the normalized rate of change of energy of turbulent fluctuations $\hat{W} = \dot{W}/P_{in}$ ($\dot{W} = -\mathrm{d}W/\mathrm{d}t$) and the sum $\hat{H} + \hat{W}$, where P_{in} is the power input into the plasma by the Langevin antenna driving. Columns from left to right are for Run 1 ($\overline{\chi} = 4.9$), Run 2 ($\overline{\chi} = 3.4$) and Run 3 ($\overline{\chi} = 1.6$).

modes; therefore, the rate of energy increase for the $k_\perp\rho_i = 20.6$ modes diminishes for $t_1 < t < t_2$. The second time scale t_2 signifies the time when this nonlinear energy loss to higher wavenumber modes increases sufficiently to balance the nonlinear energy input from lower wavenumber modes, effectively marking the saturation of a fully developed turbulent cascade.

To further illuminate the physical significance of these two time scales, we present two more measure of the turbulent cascade as a function of time. First, in figure 3(*b*), we present the time evolution of spectral index α of the one-dimensional perpendicular magnetic spectrum when fit to the functional form $C(k_\perp\rho_i)^\alpha \exp(-k_\perp\rho_e)$ with free adjustable parameters α for the spectral exponent and C as an arbitrary amplitude.

Figure 3(*c*), we plot diagnostics of the global power balance in each of the simulations. Further details of the power balance diagnostics in `AstroGK` are described in the Appendix of TenBarge *et al.* (2013), so here we present only a brief description. Energy conservation dictates that the rate of change total fluctuating power (Howes *et al.* 2006; Schekochihin *et al.* 2009) in the turbulent plasma in `AstroGK`, $\dot{W} = -\mathrm{d}W/\mathrm{d}t$, is given by $\dot{W} = P_{in} - H$, where P_{in} is the power input into the plasma by the Langevin antenna driving and H is the energy lost from the fluctuations due to collisional (and numerical) dissipation. Note that the heating $H \geqslant 0$ because collisional dissipation can only heat the plasma, removing energy irreversibly from turbulent field and plasma fluctuations and leading to thermal heating of the plasma species (which is not contained in W). In a statistically steady state, one has a time averaged $\langle\dot{W}\rangle \simeq 0$, so therefore the time-averaged antenna power input into the plasma is $\langle P_{in}\rangle \simeq \langle H\rangle \geqslant 0$, meaning that, on average, all of the input power is collisionally dissipated by the plasma. For plotting convenience, we choose to

https://doi.org/10.1017/S0022377817000319 Published online by Cambridge University Press

normalize the power balance by dividing by P_{in}, leading to a normalized expression for instantaneous energy conservation, $\hat{W} + \hat{H}$, where $\hat{W} = \dot{W}/P_{in}$ and $\hat{H} = H/P_{in}$. Energy is not conserved exactly by the `AstroGK` code due to a small amount of numerical dissipation, but the energy is typically conserved within a few per cent (TenBarge *et al.* 2013), as seen by the small departures of this sum from 1 in figure 3(*c*). Note that although the slope of the magnetic energy spectrum (figure 3*b*) has reached a steady value at t_2, the normalized heating rate $\hat{H}$ (figure 3*c*) does continue to increase after this time. Although the definition of t_2 as the saturation time of the turbulent cascade agrees qualitatively with the expected scaling with turbulent amplitude, the slight increase of energy (manifesting an increasing heating rate) after t_2 suggests that the turbulence does experience a slow evolution beyond t_2. Investigating how this slow evolution alters the properties of the turbulence will be explored in future works.

Figure 3(*b*), it is clear that second time scale t_2 is the saturation time for the development of the turbulent energy spectrum. This is the time required for the turbulent energy input at large scales to be transferred nonlinearly down to sufficiently scales that the turbulent energy is dissipated by kinetic mechanisms, irreversibly converted into plasma heat. It is interesting to note that, when normalized to the linear period t_l of the kinetic Alfvén waves that are driven at the domain scale, we generally find $t_2/t_l < 1$, in contrast to the typical time scale assumed for strong turbulence that the saturation time $t_2 \sim t_l$. The likely explanation is the dispersive nature of kinetic Alfvén waves is that in the limit $k_\perp \rho_i \gg 1$, the kinetic Alfvén wave frequency scales as $\omega \propto k_\perp \rho_i k_\parallel v_A$, meaning that smaller-scale kinetic Alfvén waves have increasingly short period when normalized to the parallel wavenumber. Therefore, the full turbulent cascade develops more rapidly than the usual expectation from the non-dispersive inertial range. This result also demonstrates that driving turbulence simulations by counterpropagating kinetic Alfvén waves is a very efficient means of generating a turbulent spectrum.

Looking at the third row of figure 3, we see that the point at which the normalized rate of energy increase in the plasma due to driving $\dot{W}/P_{in}$ is overtaken by the rate of heating due to dissipation H/P_{in} falls within the time interval $t_1 < t < t_2$. By the time t_2 is reached, the rate of heating H/P_{in} dominates over the rate of energy increase in the turbulent plasma. At $t > t_2$, eventually the time-averaged change of the turbulent plasma energy $\langle \dot{W}/P_{in} \rangle \to 0$, leaving $H/P_{in} \simeq 1$, indicating that all of the input power is collisionally dissipated, heating the plasma irreversibly.

The same qualitative behaviour of the development and saturation of the turbulent cascade is also found for cases of weak turbulence, $\chi < 1$, as shown in figure 4. Here, we plot the same rows of information as in figure 3 for Run 5 ($\overline{\chi} = 0.83$) and Run 6 ($\overline{\chi} = 0.44$). Again, two time scales are observed, a first time scale t_1 where the power-law increase of the $k_\perp \rho_i = 20.6$ decreases to a slower rate and the saturation time scale t_2 where spectral index of the perpendicular magnetic energy spectrum reaches a statistically steady value and the rate of heating H/P_{in} dominates over the rate of energy increase in the turbulent plasma $\dot{W}/P_{in}$.

For all of the Runs 1–7, the times t_1 and t_2, normalized to the linear kinetic Alfvén wave period at the domain scale (effectively the outer time scale of the turbulent cascade), are presented in table 1. For the cases of over-strong turbulence $\chi > 1$, the saturation time t_2 is relatively constant, with a value between one-quarter and one-third of the domain-scale kinetic Alfvén wave period. As the turbulence weakens in the regime $\chi < 1$, the saturation time t_2 increases monotonically as the strength of the turbulence χ decreases, as expected theoretically (Sridhar & Goldreich 1994; Howes, TenBarge & Dorland 2011*a*).

https://doi.org/10.1017/S0022377817000319 Published online by Cambridge University Press

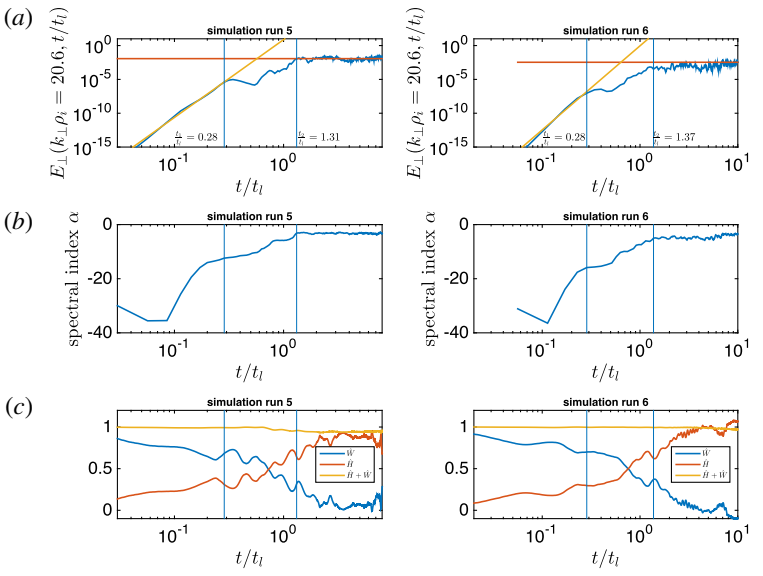

FIGURE 4. The time evolution of: (*a*) the perpendicular magnetic energy spectrum $E_\perp$ at $k_\perp\rho_i = 20$, $E_\perp$ (*a*,*b*) the spectral index α that corresponds to function $C(k_\perp\rho_i)^\alpha \exp(-k_\perp\rho_e)$ fit to $E_\perp(k_\perp)$, (*c*) the normalized total heating rate, $\hat{H} = H/P_{in}$, the normalized rate of change of energy of turbulent fluctuations $\hat{W} = \dot{W}/P_{in}$ ($\dot{W} = -\mathrm{d}W/\mathrm{d}t$) and the sum $\hat{H} + \hat{W}$, where P_{in} is the power input into the plasma by the Langevin antenna driving. Columns from left to right are for Run 5 ($\overline{\chi} = 0.83$) and Run 6 ($\overline{\chi} = 0.44$).

2.2. *Stochasticity of magnetic field lines*

Here we describe the development of the stochasticity of the magnetic field lines in gyrokinetic turbulence as a function of the time-averaged nonlinearity parameter $\overline{\chi}$. To study the magnetic field stochasticity, we employ Poincaré recurrence plots derived from snapshots of the magnetic field at different chosen times in the evolution of the turbulence simulations listed in table 1.

To construct the Poincaré plot, we begin with the magnetic field $\boldsymbol{B}(\boldsymbol{x})$ at some time t. On the perpendicular plane at one end of the simulation domain at $z = 0$, we specify a sparse pattern of points with the colour of each point creating a bullseye pattern, as shown in figure 5. The magnetic field line passing through each point is traced through the domain to the far end of the simulation domain at $z = L_\parallel$, and a point is plotted there, with colour matching that of the original field line position. That field line is periodically wrapped to $z = 0$, and the process is continued, with a coloured point plotted at each crossing at $z = L_\parallel$. We trace through the box 20 times for each field line, thereby plotting 20 coloured points on the plane for each field line. A fourth-order Runge–Kutta method with adaptive step size is used to trace each field line by integrating the ordinary differential equation $\mathrm{d}\boldsymbol{r}/\mathrm{d}l = \hat{\boldsymbol{b}}(\boldsymbol{x})$, where $\hat{\boldsymbol{b}}(\boldsymbol{x}) = \boldsymbol{B}(\boldsymbol{x})/|\boldsymbol{B}(\boldsymbol{x})|$. If the field line passes through the boundaries of the simulation domain in the x or y directions, it is periodically wrapped to the opposite boundary.

The Poincaré plots for Runs 1–4 are presented in figure 6 and for Runs 5–7 in figure 7. Stochasticity of the magnetic field is qualitatively assessed by the appearance of the Poincaré recurrence plots: a regular pattern of colours indicates a non-stochastic field, whereas a scrambling of the different colours indicates a

https://doi.org/10.1017/S0022377817000319 Published online by Cambridge University Press

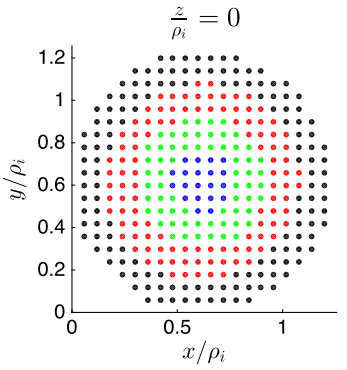

FIGURE 5. Coloured points represent the coordinates of the starting points in the $z = 0$ plane for tracing field lines to generate Poincaré recurrence plots.

stochastic field. In some cases, regions of the domain display a stochastic field while other regions appear more well ordered.

From the Poincaré plots presented in figures 6 and 7, we make the following observations. Early in the evolution at $t \ll t_2$, when the turbulence is still not well developed and little energy has cascaded to small scales to generate a broadband turbulent spectrum, the Poincaré plots for all cases show a well-ordered pattern with no indication of stochasticity. After the turbulent cascade has saturated, at times $t > t_2$, the over-strong and strong turbulence cases in Runs 1–4 with $\overline{\chi} \gtrsim 1$ all show that the magnetic field lines have become completely stochastic throughout the domain. For the weaker turbulence cases of Runs 5–7 with $\overline{\chi} < 1$, a remnant of order persists in the Poincaré plots even at $t \sim t_2$ when the turbulent cascade has saturated. At sufficiently long times $t \gg t_2$, one sees the eventual development of a fully stochastic magnetic field throughout the domain for Run 5 with $\overline{\chi} = 0.83$ and Run 6 with $\overline{\chi} = 0.44$. In contrast, the very weakest turbulence case with $\overline{\chi} = 0.14$ in Run 7 shows persistent regions of order, even at long times $t > 10t_2$. Therefore, it seems that there is indeed a minimum amplitude threshold χ_{thresh} for the development of a completely stochastic magnetic field within the saturation time interval $t_2 < t < 13t_2$, with order persisting for cases with nonlinear parameters $\chi \lesssim \chi_{thresh} \sim 0.1$.

2.3. *Separation of the magnetic field lines*

The stochasticity is not the only feature that characterizes the magnetic field line wander in plasma turbulence. Two adjacent magnetic field lines may also separate from one another as we follow along one of the field lines. This magnetic field line separation may significantly impact the propagation of energetic particles in a turbulent plasma. Here we investigate the separation of stochastic magnetic field lines caused by plasma turbulence as a function of the nonlinearity parameter χ using gyrokinetic simulations (listed in table 1). We consider only Runs 1–6, excluding Run 7 as the magnetic field lines are not fully stochastic at the saturation phase of that simulation run.

To explore the separation of magnetic field lines, we assume an extended domain built up from the periodic extension of the single gyrokinetic simulation domain of size $L_\perp \times L_\perp \times L_\parallel$. The magnetic field is initially defined by simulation over the ranges $0 \leqslant z \leqslant L_\parallel$ and $0 \leqslant x, y \leqslant L_\perp$. To track the magnetic field lines in the extended

https://doi.org/10.1017/S0022377817000319 Published online by Cambridge University Press

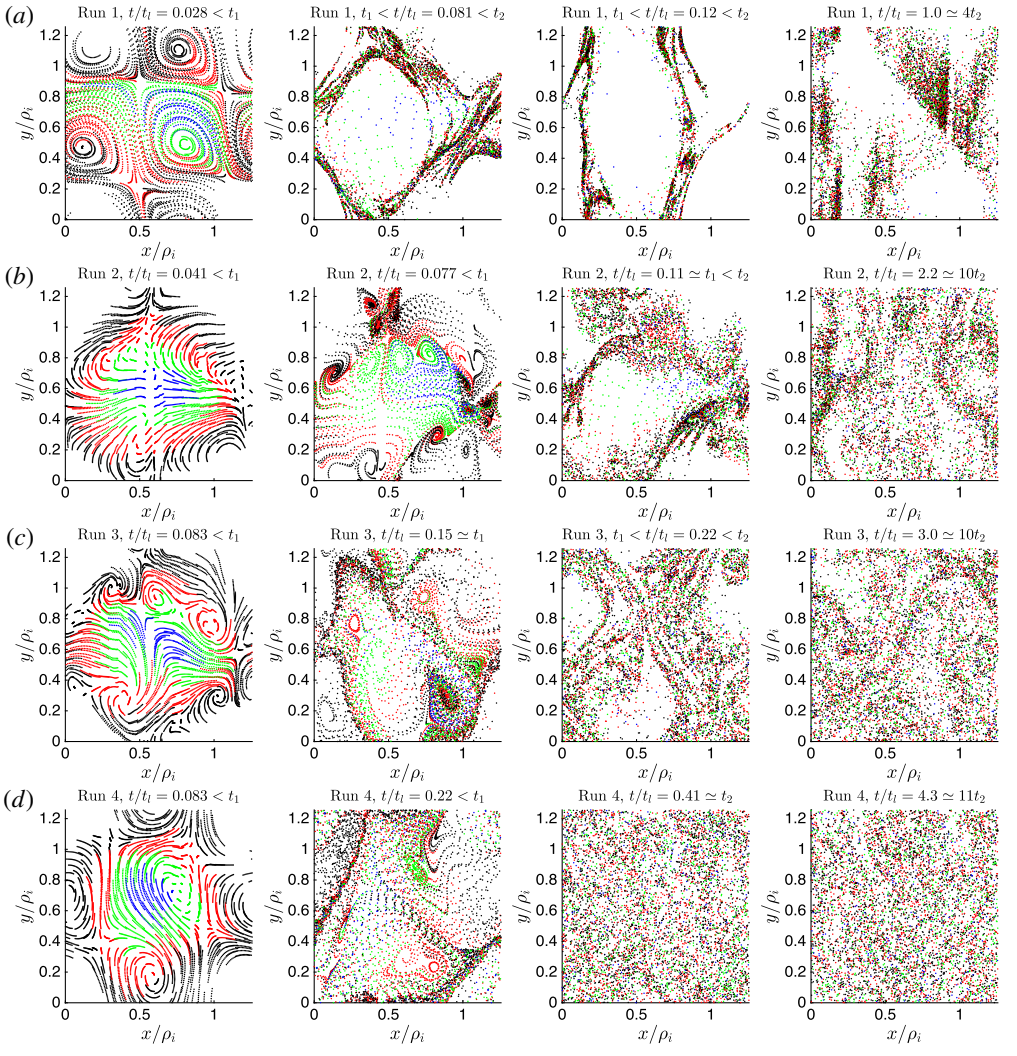

FIGURE 6. Poincaré recurrence plots for over-strong and strong turbulence in Runs 1–4 at the times indicated. The corresponding time-averaged nonlinearity parameters are $\overline{\chi} = 4.9$ (a), $\overline{\chi} = 3.4$ (b), $\overline{\chi} = 1.6$ (c) and $\overline{\chi} = 1.3$ (d).

spatial domain beyond these limits, we begin at a point in the $z = 0$ plane and trace along the magnetic field line passing through that point (using the fourth-order Runge–Kutta method with adaptive step size) in the $+\hat{z}$ direction. When the field line reaches the end of the single simulation domain at $z = L_\parallel$, it enters an identical domain periodically extended to $z > L_\parallel$, as depicted in figure 8. If the magnetic field line exits through the side of the domain at $x, y < 0$ or $x, y > L_\perp$, it is not periodically wrapped to the opposite side but instead extended into a periodically continued extended domain in the same direction, as shown in figure 8. To be clear, the vector magnetic field in each of the six rectangular black boxes in figure 8 is identical, derived from a single time snapshot of the gyrokinetic simulation.

To investigate the separation of magnetic field lines, we initially select a large number of field lines uniformly distributed within a circular region in (x, y) plane at

https://doi.org/10.1017/S0022377817000319 Published online by Cambridge University Press

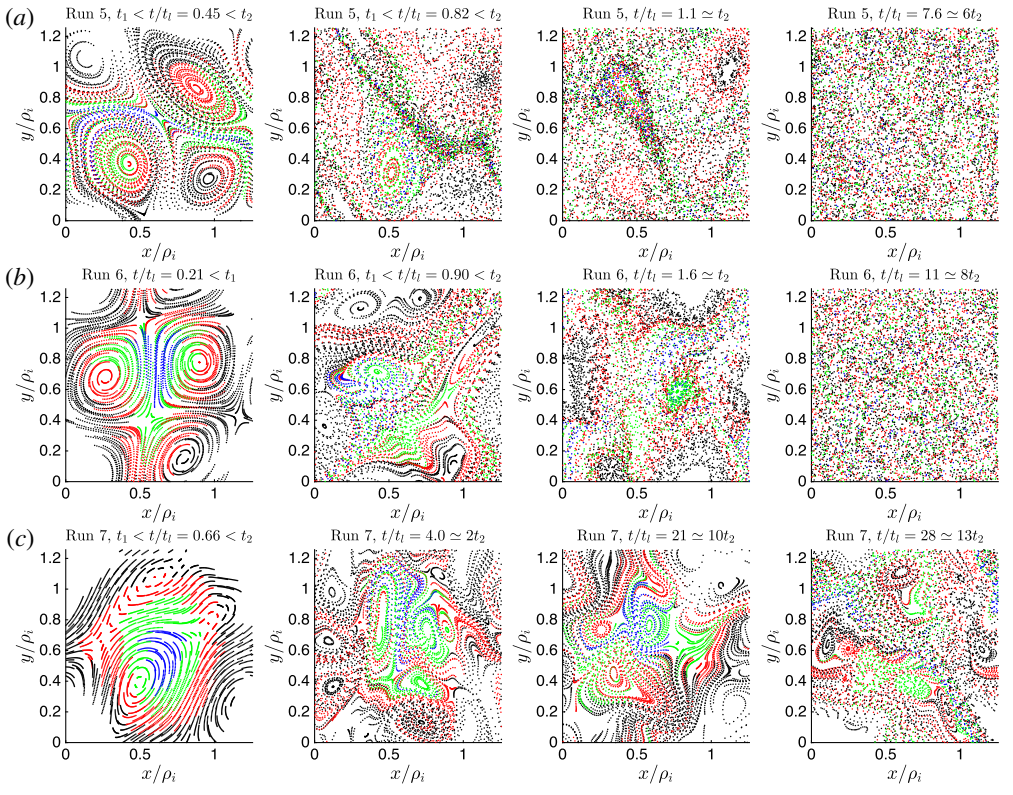

FIGURE 7. Poincaré recurrence plots for weak turbulence in Runs 5–7 at the times indicated. The corresponding time-averaged nonlinearity parameters are $\overline{\chi} = 0.83$ (*a*), $\overline{\chi} = 0.44$ (*b*) and $\overline{\chi} = 0.14$ (*c*).

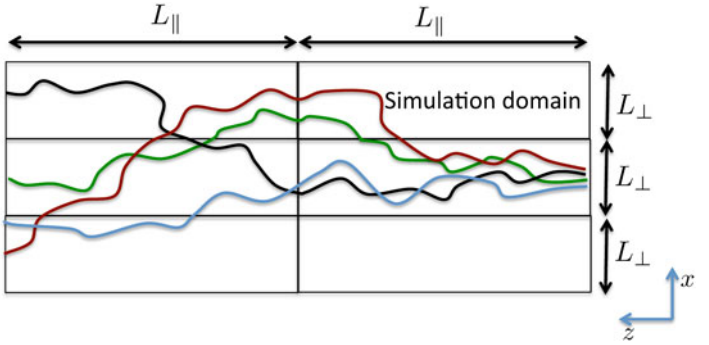

FIGURE 8. Sketch describing how field lines pass through an extended domain built of six simulation boxes, showing the tracing of several wandering magnetic field lines up to distance $z = 2L_\parallel$.

$z = 0$, (their uniform distribution is depicted in side projection in figure 9*c*). These field lines are each followed through the extended simulation box (figure 9*b*), after which their distribution appears to be well fit by a Gaussian distribution (figure 9*a*, blue line) at $z = 3L_\parallel$. The full width at half-maximum (FWHM) of the Gaussian

https://doi.org/10.1017/S0022377817000319 Published online by Cambridge University Press

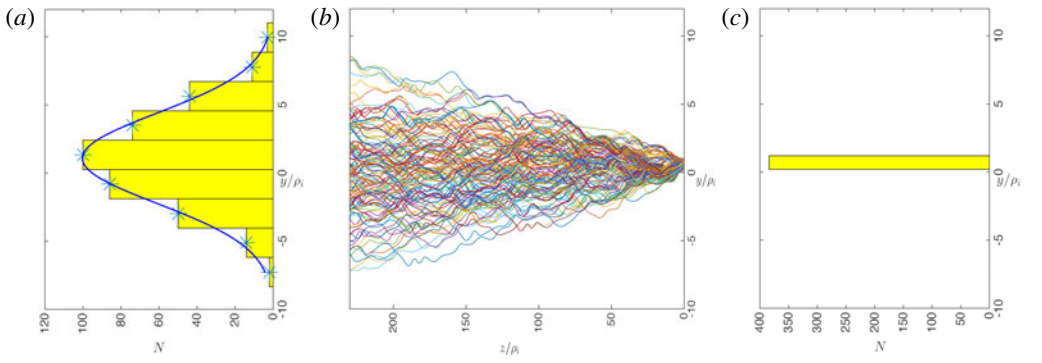

FIGURE 9. An initially uniform distribution of field lines within a small circle in the plane at $z=0$ (c) wanders through the simulation domain in Run 3 (b) to generate a Gaussian distribution at $z=3L_{\parallel}$ (a).

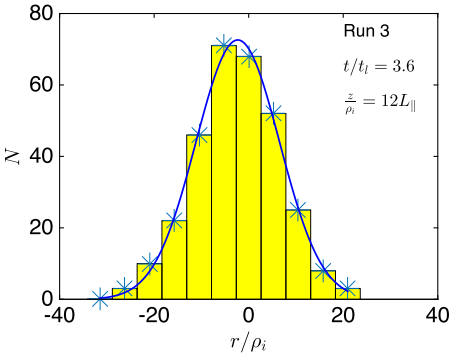

FIGURE 10. For Run 3 with $\overline{\chi}=1.6$, the binned distribution of the field lines (asterisks) at $z=12L_{\parallel}$ versus the normalized separation length r/ρ_i, where $r=\sqrt{x^2+y^2}$. The separation distance is divided into 11 bins. The distribution is fit to a Gaussian function with a FWHM $\langle \delta r \rangle$.

function represents the mean separation $\langle(\delta r)\rangle$ of the field line at given distance $z=n\times L_{\parallel}$. For example, in figure 10 we plot the distribution of the field lines (stars) in (x, y) plane at $z=12L_{\parallel}$ for Run 3 (at time $t/t_l=3.6$), showing that the distribution of the field lines is well fit by a Gaussian function (blue solid line). Here it is worth mentioning that the centre of the ensemble of the field lines in the x–y plane is changing with distance z. The centre position of the field lines at a given distance z can be calculated as the average of all field line positions in x–y plane at distance z. The distributions of the field lines (see, e.g. figures 9 and 10) are estimated with respect to this moving centre. In our analysis we focus only on the spread of the magnetic field lines.

Using this method to trace the magnetic field line separation for Runs 1–6 in table 1, we compute directly the mean square displacement $\langle(\delta r)^2\rangle$ as a function of $z/L_{\parallel}$ at different evolution times within the saturation phase of each simulation run. Note the we do not fit the FWHM of the best fit Gaussian, but rather calculate directly the mean square displacement $\langle(\delta r)^2\rangle$ of the magnetic field line distribution in order to account for any skewness in the resulting distribution that may prevent a good

https://doi.org/10.1017/S0022377817000319 Published online by Cambridge University Press

Gaussian fit. We fit the computed mean square displacement $\langle(\delta r)^2\rangle$ by the power-law function

$$\langle(\delta r)^2\rangle = A(z/L_\parallel)^p, \tag{2.2}$$

where we expect the amplitude factor $A(\chi)$ and the power-law exponent $p(\chi)$ both to be a function of the nonlinearity parameter χ. Note that an exponent of $p = 1$ corresponds to a diffusive behaviour of the field line separation, while $p > 1$ indicates a superdiffusive process and $p < 1$ indicates a subdiffusive process.

In figure 11, we plot the results of this analysis of the magnetic field line separation, including the values of the fitting parameters A and p. For each simulation run, we plot the results of $\langle(\delta r)^2\rangle$ as a function of the distance along the equilibrium magnetic field $z/L_\parallel$ at four different representative times after the turbulent cascade has saturated. Note that, in addition to the time-averaged nonlinearity parameter $\overline{\chi}$ given for each run in table 1, we also compute the instantaneous nonlinearity parameter χ at each of the chosen times in figure 11.

From the results in figure 11, we find the following general properties about the separation of magnetic fields lines as a function of the turbulence amplitudes χ. First, the amplitude of the field line separation, parameterized by the coefficient A, generally increases monotonically with the time-averaged nonlinearity parameter $\overline{\chi}$. However, it does not always follow that a larger instantaneous value of the nonlinearity parameter χ will yield a larger value of the coefficient A. This finding suggests that the amplitude of the field line separation may indeed depend not only on the nonlinearity parameter, but also on the history of the turbulent tangling of the magnetic field. Therefore, to determine the functional forms of the amplitude $A(\chi)$ and the power-law exponent $p(\chi)$ requires a statistical approach, effectively leading us to determine averaged values of these parameters as a function of the averaged nonlinearity parameter, $\overline{A}(\overline{\chi})$ and $\overline{p}(\overline{\chi})$.

Another important conclusion regards the power-law scaling exponent p of the field line separation as a function of the nonlinearity parameter χ. Again, in general, we find a larger exponent p for larger values of the time-averaged nonlinearity parameter $\overline{\chi}$. For the cases of over-strong and strong turbulence in Runs 1–4 with $\overline{\chi} > 1$, the field line separation appears to follow a superdiffusive scaling, $p > 1$, as a function of z; in contrast, for the weak turbulence cases Runs 5 and 6, it follows a subdiffusive scaling, $p < 1$.

To quantitatively describe the field line separation as a function of the time-averaged nonlinearity parameter $\overline{\chi}$, we compute the mean values of the amplitude coefficient $\overline{A}$ and the exponent $\overline{p}$ for each of the simulation Runs 1–6. We compute the mean and standard deviation for $\overline{A}$ and $\overline{p}$ by averaging over the four values of p and A shown in figure 11. We plot in figure 12 the average values $\overline{A}$ (*a*) and $\overline{p}$ (*b*) as a function of the time-averaged nonlinearity parameter $\overline{\chi}$. Uncertainties in figure 12 are given by the standard deviation of each of these averaged quantities.

Figure 12(*a*) clearly shows that $\overline{A}$ nonlinearly increases with increasing $\overline{\chi}$ indicating more spreading of magnetic field in strong turbulence than in weak turbulence. The data are fit to an exponential form

$$\overline{A}(\overline{\chi}) = \overline{a}_0 \exp(\overline{b}_0\overline{\chi}), \tag{2.3}$$

with best fit values $\overline{a}_0 = 0.3$ and $\overline{b}_0 = 1.1$.

Figure 12(*b*) displays the dependence of the mean exponent $\overline{p}$ on the time-averaged nonlinearity parameter $\overline{\chi}$. We fit this behaviour to the functional form

$$\overline{p}(\overline{\chi}) = \overline{p}_0 - \overline{p}_1 \exp C_1\overline{\chi}, \tag{2.4}$$

https://doi.org/10.1017/S0022377817000319 Published online by Cambridge University Press

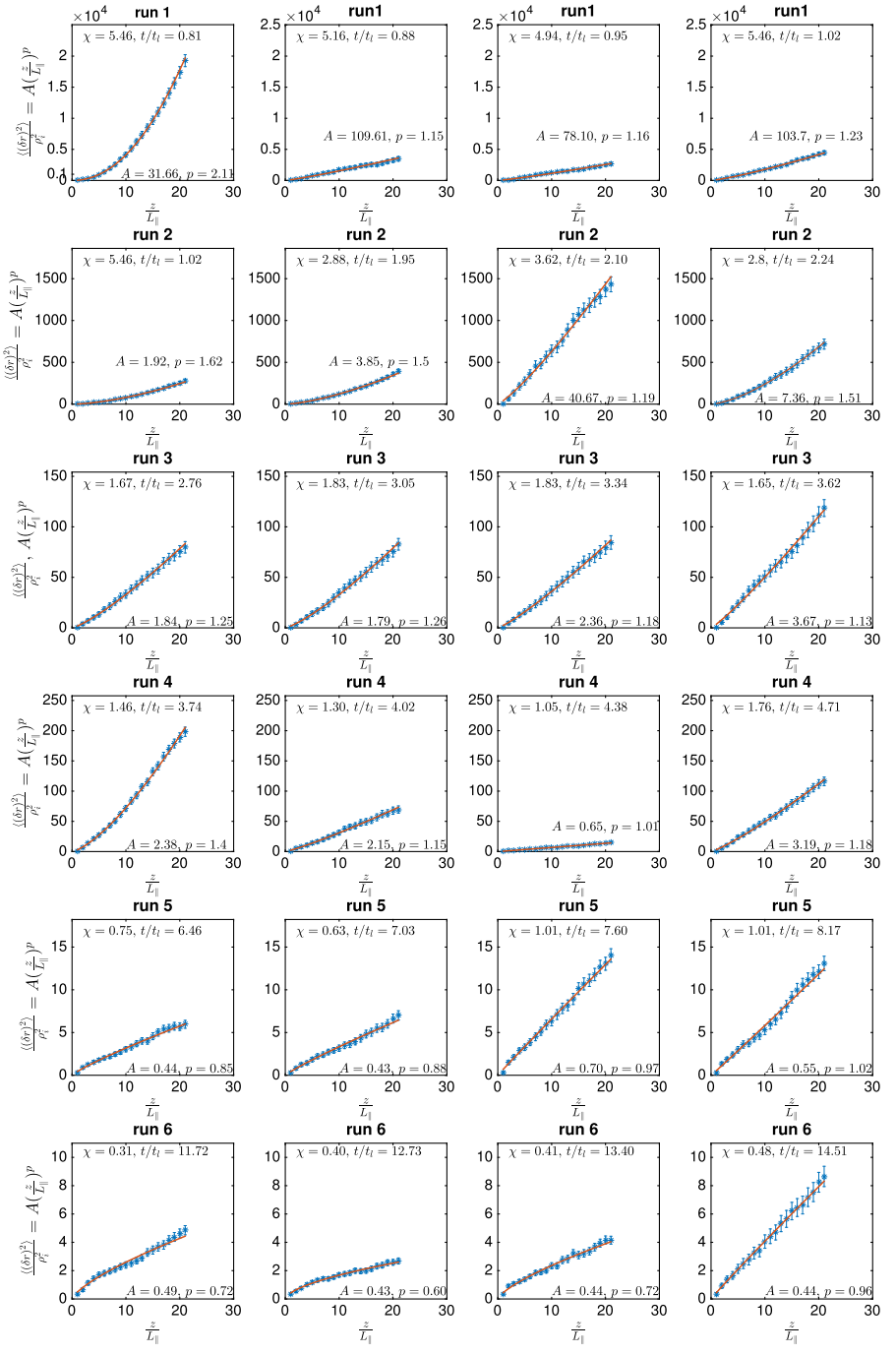

FIGURE 11. For Runs 1–6, plots of the mean square separation $\langle \delta r^2 \rangle$ versus distance $z/L_\parallel$ at four different evolution times. The solid curves are the corresponding power-law fitting functions, with coefficients denoted.

https://doi.org/10.1017/S0022377817000319 Published online by Cambridge University Press

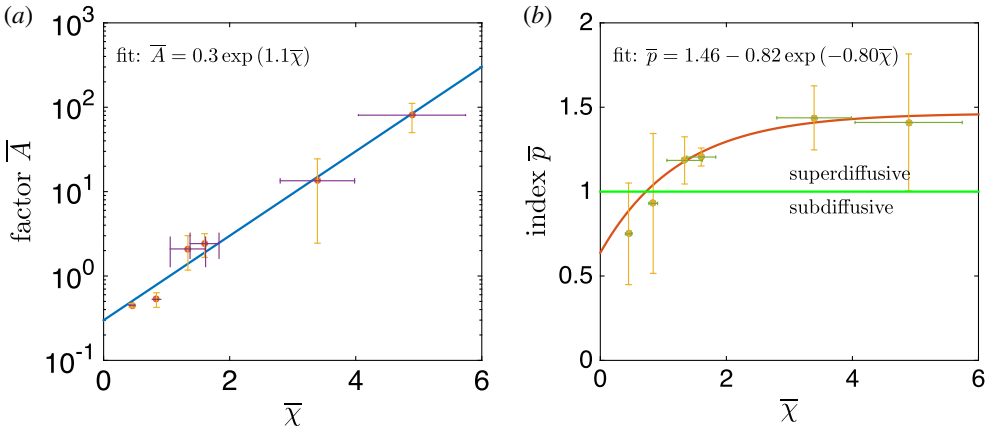

FIGURE 12. (*a*) The mean value of the amplitude coefficient $\overline{A}$ versus the time-averaged nonlinearity parameter $\overline{\chi}$. The blue line is the corresponding power-law exponent fitting curve $\overline{A}(\overline{\chi}) = 0.3\exp(1.1\overline{\chi})$. (*b*) The average value of exponent $\overline{p}$ versus the time-averaged nonlinearity parameter $\overline{\chi}$. The red line is the corresponding fitting curve $\overline{p} = 1.46 - 0.82\exp(-0.80\overline{\chi})$. The green horizontal line corresponds to value $\overline{p} = 1$ which is associated with a standard diffusive process. Vertical and horizontal error bars correspond to standard deviations.

where the best fit yields values $\overline{p}_0 = 1.46$, $\overline{p}_1 = 0.82$ and $C_1 = -0.80$. Based on this statistically averaged functional form, we conclude that the diffusion approximation is a reasonable model for turbulence with a nonlinearity parameter $\overline{\chi} = 1. \pm 0.15$.

3. Discussion and conclusions

In this investigation, we have explored the saturation of the turbulent cascade, the development of stochasticity due to turbulent tangling of the magnetic field lines and the separation of field lines through the turbulent dynamics using nonlinear gyrokinetic simulations of weakly collisional plasma turbulence, relevant to many turbulent space and astrophysical plasma environments. We focus on the sub-ion range of kinetic Alfvén wave turbulence, corresponding to the dissipation range of turbulence in the solar wind, over the range $5 \leqslant k_\perp \rho_i \leqslant 105$, or $0.12 \leqslant k_\perp \rho_e \leqslant 2.5$. The motivation for beginning this methodical investigation of magnetic field line wander in plasma turbulence with the small-scale end of the turbulent spectrum is that the kinetic physical mechanisms, including collisionless damping and collisionless magnetic reconnection, are resolved properly by our gyrokinetic simulations as long as we resolve wavenumbers $k_\perp \rho_e \sim 2$ (Howes *et al.* 2006; Numata *et al.* 2010; TenBarge *et al.* 2013). Our focus is to understand the properties of magnetic field line wander as a function of the amplitude of the turbulence, parameterized here by the dimensionless nonlinearity parameter χ, approximately a measure of the linear wave period to the nonlinear energy transfer time scale. We perform here a set of seven simulations with time-averaged nonlinearity parameter $\overline{\chi}$ varying from over-strong turbulence with $\overline{\chi} = 4.9$, to critically balance, strong turbulence with $\overline{\chi} = 1.3$ to weak turbulence with $\overline{\chi} = 0.14$.

First, we have investigated the development and saturation of the turbulent cascade, beginning with uniform, straight magnetic field conditions driven by an antenna

https://doi.org/10.1017/S0022377817000319 Published online by Cambridge University Press

that creates counterpropagating kinetic Alfvén waves at the domain scale. Nonlinear interactions between the counterpropagating kinetic Alfvén waves efficiently transfer energy to small scales, generating a broadband turbulent cascade of magnetic field and plasma bulk flow fluctuations. For all values of $\overline{\chi}$, we find the development of the cascade is characterized by two time scales t_1 and t_2. At time t_1, the small-scale modes reach sufficient amplitudes to interact nonlinearly and transfer their energy to yet smaller-scale modes. In the time interval, $t_1 < t < t_2$, the normalized rate of energy increase in the plasma due to driving $\dot{W}/P_{in}$ is overtaken by the rate of heating due to dissipation H/P_{in}, indicating the approach to saturation. At the saturation time t_2, the spectral index of the perpendicular magnetic energy spectrum α reaches a statistically steady value and the rate of heating H/P_{in} dominates over the rate of energy increase in the turbulent plasma $\dot{W}/P_{in}$, indicating that all of the input power is collisionally dissipated, heating the plasma irreversibly.

Next, we have studied the development of stochasticity of the magnetic field lines as a function of the time-averaged nonlinearity parameter $\overline{\chi}$ using Poincaré recurrence plots. We find that for over-strong and strong turbulence cases with $\overline{\chi} \gtrsim 1$, the magnetic field lines have become completely stochastic throughout the domain for $t \geqslant t_2$. For weaker turbulence cases with $\overline{\chi} < 1$, a remnant of order persists in the Poincaré plots even at $t \sim t_2$ when the turbulent cascade has saturated. Over a much longer time $t \gg t_2$, the turbulent magnetic field lines become fully stochastic if the turbulent amplitude exceeds a threshold value $\chi_{thresh} \sim 0.1$. For yet weaker turbulence with $\chi \lesssim 0.1$, ordered regions of simulation domain persist, indicating that a fully stochastic magnetic field does not arise below this amplitude threshold over the course of the saturation time interval $t_2 < t < 13t_2$.

Finally, we quantified the mean square displacement of magnetic field lines in the turbulent magnetic field with a functional form $\langle(\delta r)^2\rangle = A(z/L_\parallel)^p$, where we expect the amplitude factor $A(\chi)$ and the power-law exponent $p(\chi)$ both to be a function of the nonlinearity parameter χ. Statistical determinations of these two parameters yield the best fit results for the amplitude coefficient $\overline{A}(\overline{\chi}) = \overline{a}_0 \exp(\overline{b}_0\overline{\chi})$ for $0.14 \leqslant \overline{\chi} \leqslant 4.9$ (with $\overline{a_0} = 0.3$, and $\overline{b_0} = 1.1$) and the power-law exponent $\overline{p}(\overline{\chi}) = \overline{p}_0 - \overline{p}_1 \exp C_1\overline{\chi}$ with $\overline{p}_0 = 1.46$, $\overline{p}_1 = 0.82$ and $C_1 = -0.80$, as shown in figure 12.

The analysis of magnetic field stochasticity using Poincaré plots for the magnetic field tracing has been also used in plasma fusions (Wang *et al.* 2011; Pueschel *et al.* 2013). For example, Pueschel *et al.* (2013) have implemented the radial displacement of the field lines as a function of the number of poloidal turns to estimate the field line diffusivity. The authors found that the magnetic field lines follow a diffusive law after a few tens of poloidal turns. Although the geometry of the background field in our analysis is different from the one used in the work of Pueschel *et al.* (2013), we also found that the field lines may obey a diffusive law in gyrokinetic turbulence if the nonlinearity parameter is approximately 1 as shown in figure 12.

Furthermore, studies of the effect of magnetic field stochasticity on zonal flows in plasma fusion have shown that the normalized critical value β_{crit}^{NZT} of the electron normalized plasma pressure for non-zonal transition (NZT) depends on the amplitude of the magnetic field fluctuations (see e.g. Pueschel *et al.* 2014). The authors found that a strong driving (or higher background gradients) leads to higher radial displacement of magnetic field lines as a result of magnetic field stochasticity. As a consequence, the NZT can occur for relatively smaller values of β_{crit}^{NZT}. The increase in the turbulence amplitude will cause more separation of the magnetic field lines in gyrokinetic turbulence as found in our paper.

The nonlinearity parameter was also found to be a crucial for development of the magnetic field wander in MHD turbulence. It has been demonstrated that the magnetic

https://doi.org/10.1017/S0022377817000319 Published online by Cambridge University Press

stochasticity in weak MHD turbulence (when the nonlinearity parameter is less than 1) does not fully develop (Eyink, Lazarian & Vishniac 2011). However, as the turbulent cascade proceeds and the nonlinearity parameter is close to unity, the spontaneous stochasticity of magnetic field lines is induced in MHD turbulence and the rate of magnetic reconnection is altered (Eyink 2011).

As mentioned above, to better describe the energetic particle propagation we need a realistic model of turbulence and an accurate transport theory. If we assume that the gyrocentres of the energetic charged particles follow magnetic field lines then the cross-field transport of these particles is governed by the perpendicular spread of magnetic field lines. In this limit, if the magnetic field lines are diffusive, then the perpendicular diffusion coefficient of the energetic particles can be given as $\kappa_\perp = vD_{FL}$ (Jokipii 1966), where $D_{FL} = \langle(\delta r)^2\rangle/2z$ is the magnetic field diffusion coefficient and v is the velocity of the energetic particles. For instance, in our analysis we found that the magnetic field lines are nearly diffusive in critically balance gyrokinetic turbulence (when $\overline{\chi} = 1$), and we get $D_{FL} = \langle(\delta r)^2\rangle/2z \simeq \rho_i^2\overline{A}(\overline{\chi} = 1)/L_\parallel$, and thus the particle cross-field transport coefficient $\kappa_\perp \simeq v\rho_i^2\overline{A}/2L_\parallel$. In this case, the value of D_{FL} is approximately 0.3 in units of $L_\perp^2/L_\parallel$ (with $L_\perp = 2\pi\rho_i/5$) when $\overline{\chi} = 1$ in gyrokinetic turbulence simulation. This value is close to the one of $D_{FL} \simeq 0.33$ estimated for critically balance reduced MHD turbulence (Ruffolo & Matthaeus 2013; Snodin *et al.* 2013).

In heliospheric plasma, the diffusion of the solar energetic particles in the interplanetary medium is affected by solar wind turbulence. During their transit from the Sun's atmosphere to the outer heliosphere the solar energetic particles go through varying conditions of solar wind plasma, for example, the plasma β and the ratio ion-to-electron temperature T_i/T_e vary with heliocentric distance. The variation of these plasma parameters can be crucial for the amount of the perpendicular displacement of the magnetic field lines. For instance, in fusion plasmas, it has been shown that the related stochasticity parameter varies with respect to the plasma β in gyrokinetic turbulence in CYCLONE base case plasmas Pueschel *et al.* (2013).

In the future work, we will employ direct numerical simulations of plasma turbulence to determine how the properties of the magnetic field line wander vary with the plasma parameters, such as the plasma β and T_i/T_e (as the turbulence dissipation and magnetic reconnection strongly depend on these plasma parameters), and with the parameters of the turbulence, such as the length scale range characterized by $k_{\perp 0}\rho_i$.

Acknowledgements

The work has been supported by NSF CAREER Award AGS-1054061 and NASA NNX10AC91G.

REFERENCES

ABEL, I. G., BARNES, M., COWLEY, S. C., DORLAND, W. & SCHEKOCHIHIN, A. A. 2008 Linearized model Fokker–Planck collision operators for gyrokinetic simulations. I. Theory. *Phys. Plasmas* **15** (12), 122509.

ALEXANDROVA, O., LACOMBE, C., MANGENEY, A., GRAPPIN, R. & MAKSIMOVIC, M. 2012 Solar wind turbulent spectrum at plasma kinetic scales. *Astrophys. J.* **760**, 121.

BARNES, M., ABEL, I. G., DORLAND, W., ERNST, D. R., HAMMETT, G. W., RICCI, P., ROGERS, B. N., SCHEKOCHIHIN, A. A. & TATSUNO, T. 2009 Linearized model Fokker–Planck collision operators for gyrokinetic simulations. II. Numerical implementation and tests. *Phys. Plasmas* **16** (7), 072107.

https://doi.org/10.1017/S0022377817000319 Published online by Cambridge University Press

Beresnyak, A. 2013 Asymmetric diffusion of magnetic field lines. *Astrophys. J.* **767**, L39 4 pp.

Bieber, J. W., Wanner, W. & Matthaeus, W. H. 1996 Dominant two-dimensional solar wind turbulence with implications for cosmic ray transport. *J. Geophys. Res.* **101**, 2511–2522.

Biskamp, D., Schwarz, E. & Drake, J. F. 1996 Two-dimensional electron magnetohydrodynamic turbulence. *Phys. Rev. Lett.* **76**, 1264–1267.

Biskamp, D., Schwarz, E., Zeiler, A., Celani, A. & Drake, J. F. 1999 Electron magnetohydrodynamic turbulence. *Phys. Plasmas* **6**, 751–758.

Boldyrev, S. 2006 Spectrum of magnetohydrodynamic turbulence. *Phys. Rev. Lett.* **96** (11), 115002.

Cho, J. & Lazarian, A. 2004 The anisotropy of electron magnetohydrodynamic turbulence. *Astrophys. J. Lett.* **615**, L41–L44.

Cho, J. & Lazarian, A. 2009 Simulations of electron magnetohydrodynamic turbulence. *Astrophys. J.* **701**, 236–252.

Cho, J. & Vishniac, E. T. 2000 The anisotropy of magnetohydrodynamic Alfvénic turbulence. *Astrophys. J.* **539**, 273–282.

Drake, D. J., Schroeder, J. W. R., Howes, G. G., Kletzing, C. A., Skiff, F., Carter, T. A. & Auerbach, D. W. 2013 Alfvén wave collisions, the fundamental building block of plasma turbulence. IV. Laboratory experiment. *Phys. Plasmas* **20** (7), 072901.

Eyink, G. L. 2011 Stochastic flux freezing and magnetic dynamo. *Phys. Rev.* E **83** (5), 056405.

Eyink, G. L., Lazarian, A. & Vishniac, E. T. 2011 Fast magnetic reconnection and spontaneous stochasticity. *Astrophys. J.* **743**, 51.

Frieman, E. A. & Chen, L. 1982 Nonlinear gyrokinetic equations for low-frequency electromagnetic waves in general plasma equilibria. *Phys. Fluids* **25**, 502–508.

Galtier, S., Nazarenko, S. V., Newell, A. C. & Pouquet, A. 2000 A weak turbulence theory for incompressible magnetohydrodynamics. *J. Plasma Phys.* **63**, 447–488.

Ghosh, S. & Goldstein, M. L. 1997 Anisotropy in Hall MHD turbulence due to a mean magnetic field. *J. Plasma Phys.* **57**, 129–154.

Goldreich, P. & Sridhar, S. 1995 Toward a theory of interstellar turbulence II. Strong Alfvénic turbulence. *Astrophys. J.* **438**, 763–775.

Guest, B. & Shalchi, A. 2012 Random walk of magnetic field lines in dynamical turbulence: a field line tracing method. II. Two-dimensional turbulence. *Phys. Plasmas* **19** (3), 032902.

Haas, F. A. & Thyagaraja, A. 1986 Conceptual and experimental bases of theories of anomalous transport in tokamaks. *Phys. Rep.* **143**, 241–276.

Hatch, D. R., Pueschel, M. J., Jenko, F., Nevins, W. M., Terry, P. W. & Doerk, H. 2012 Origin of magnetic stochasticity and transport in plasma microturbulence. *Phys. Rev. Lett.* **108** (23), 235002.

Hatch, D. R., Pueschel, M. J., Jenko, F., Nevins, W. M., Terry, P. W. & Doerk, H. 2013 Magnetic stochasticity and transport due to nonlinearly excited subdominant microtearing modes. *Phys. Plasmas* **20** (1), 012307.

Howes, G. G., Cowley, S. C., Dorland, W., Hammett, G. W., Quataert, E. & Schekochihin, A. A. 2006 Astrophysical gyrokinetics: basic equations and linear theory. *Astrophys. J.* **651**, 590–614.

Howes, G. G., Dorland, W., Cowley, S. C., Hammett, G. W., Quataert, E., Schekochihin, A. A. & Tatsuno, T. 2008*b* Kinetic simulations of magnetized turbulence in astrophysical plasmas. *Phys. Rev. Lett.* **100** (6), 065004–+.

Howes, G. G., Drake, D. J., Nielson, K. D., Carter, T. A., Kletzing, C. A. & Skiff, F. 2012 Toward astrophysical turbulence in the laboratory. *Phys. Rev. Lett.* **109** (25), 255001.

Howes, G. G. & Nielson, K. D. 2013 Alfvén wave collisions, the fundamental building block of plasma turbulence. I. Asymptotic solution. *Phys. Plasmas* **20** (7), 072302.

Howes, G. G., Nielson, K. D., Drake, D. J., Schroeder, J. W. R., Skiff, F., Kletzing, C. A. & Carter, T. A. 2013 Alfvén wave collisions, the fundamental building block of plasma turbulence. III. Theory for experimental design. *Phys. Plasmas* **20** (7), 072304.

Howes, G. G., TenBarge, J. M. & Dorland, W. 2011*a* A weakened cascade model for turbulence in astrophysical plasmas. *Phys. Plasmas* **18** (10), 102305.

HOWES, G. G., TENBARGE, J. M., DORLAND, W., QUATAERT, E., SCHEKOCHIHIN, A. A., NUMATA, R. & TATSUNO, T. 2011*b* Gyrokinetic simulations of solar wind turbulence from ion to electron scales. *Phys. Rev. Lett.* **107** (3), 035004.

IROSHNIKOV, P. S. 1963 Turbulence of a conducting fluid in a strong magnetic field. *Astron. Zh.* **40**, 742–+.

JOKIPII, J. R. 1966 Cosmic-ray propagation. I. Charged particles in a random magnetic field. *Astrophys. J.* **146**, 480.

JOKIPII, J. R. & PARKER, E. N. 1968 Random walk of magnetic lines of force in astrophysics. *Phys. Rev. Lett.* **21**, 44–47.

KRAICHNAN, R. H. 1965 Inertial-range spectrum of hydromagnetic turbulence. *Phys. Fluids* **8**, 1385–1387.

KROMMES, J. A., OBERMAN, C. & KLEVA, R. G. 1983 Plasma transport in stochastic magnetic fields. Part 3. Kinetics of test particle diffusion. *J. Plasma Phys.* **30**, 11–56.

LAVAL, G. 1993 Particle diffusion in stochastic magnetic fields. *Phys. Fluids* B **5**, 711–721.

LAZARIAN, A. & VISHNIAC, E. T. 1999 Reconnection in a weakly stochastic field. *Astrophys. J.* **517**, 700–718.

LAZARIAN, A., VISHNIAC, E. T. & CHO, J. 2004 Magnetic field structure and stochastic reconnection in a partially ionized gas. *Astrophys. J.* **603**, 180–197.

LAZARIAN, A. & YAN, H. 2014 Superdiffusion of cosmic rays: implications for cosmic ray acceleration. *Astrophys. J.* **784**, 38.

MARON, J., CHANDRAN, B. D. & BLACKMAN, E. 2004 Divergence of neighboring magnetic-field lines and fast-particle diffusion in strong magnetohydrodynamic turbulence, with application to thermal conduction in galaxy clusters. *Phys. Rev. Lett.* **92** (4), 045001.

MARON, J. & GOLDREICH, P. 2001 Simulations of incompressible magnetohydrodynamic turbulence. *Astrophys. J.* **554**, 1175–1196.

MATTHAEUS, W. H., GRAY, P. C., PONTIUS, D. H. JR & BIEBER, J. W. 1995 Spatial structure and field-line diffusion in transverse magnetic turbulence. *Phys. Rev. Lett.* **75**, 2136–2139.

MATTHAEUS, W. H., OUGHTON, S., GHOSH, S. & HOSSAIN, M. 1998 Scaling of anisotropy in hydromagnetic turbulence. *Phys. Rev. Lett.* **81**, 2056–2059.

MONTGOMERY, D. & MATTHAEUS, W. H. 1995 Anisotropic modal energy transfer in interstellar turbulence. *Astrophys. J.* **447**, 706.

MONTGOMERY, D. & TURNER, L. 1981 Anisotropic magnetohydrodynamic turbulence in a strong external magnetic field. *Phys. Fluids* **24**, 825–831.

NEVINS, W. M., WANG, E. & CANDY, J. 2011 Magnetic stochasticity in gyrokinetic simulations of plasma microturbulence. *Phys. Rev. Lett.* **106** (6), 065003.

NIELSON, K. D., HOWES, G. G. & DORLAND, W. 2013 Alfvén wave collisions, the fundamental building block of plasma turbulence. II. Numerical solution. *Phys. Plasmas* **20** (7), 072303.

NUMATA, R., HOWES, G. G., TATSUNO, T., BARNES, M. & DORLAND, W. 2010 AstroGK: astrophysical gyrokinetics code. *J. Comput. Phys.* **229**, 9347–9372.

OUGHTON, S., PRIEST, E. R. & MATTHAEUS, W. H. 1994 The influence of a mean magnetic field on three-dimensional magnetohydrodynamic turbulence. *J. Fluid Mech.* **280**, 95–117.

PUESCHEL, M. J., HATCH, D. R., GÖRLER, T., NEVINS, W. M., JENKO, F., TERRY, P. W. & TOLD, D. 2013 Properties of high-β microturbulence and the non-zonal transition. *Phys. Plasmas* **20** (10), 102301.

PUESCHEL, M. J., TERRY, P. W. & HATCH, D. R. 2014 Aspects of the non-zonal transitiona. *Phys. Plasmas* **21** (5), 055901.

QIN, G. & SHALCHI, A. 2013 The role of the Kubo number in two-component turbulence. *Phys. Plasmas* **20** (9), 092302.

RAGOT, B. R. 2011 Statistics of field-line dispersal: random-walk characterization and supradiffusive regime. *Astrophys. J.* **728**, 50.

RECHESTER, A. B. & ROSENBLUTH, M. N. 1978 Electron heat transport in a tokamak with destroyed magnetic surfaces. *Phys. Rev. Lett.* **40**, 38–41.

RUFFOLO, D. & MATTHAEUS, W. H. 2013 Theory of magnetic field line random walk in noisy reduced magnetohydrodynamic turbulence. *Phys. Plasmas* **20** (1), 012308.

SAHRAOUI, F., GOLDSTEIN, M. L., ROBERT, P. & KHOTYAINTSEV, Y. V. 2009 Evidence of a cascade and dissipation of solar-wind turbulence at the electron gyroscale. *Phys. Rev. Lett.* **102** (23), 231102–+.

SCHEKOCHIHIN, A. A., COWLEY, S. C., DORLAND, W., HAMMETT, G. W., HOWES, G. G., QUATAERT, E. & TATSUNO, T. 2009 Astrophysical gyrokinetics: kinetic and fluid turbulent cascades in magnetized weakly collisional plasmas. *Astrophys. J. Suppl. Ser.* **182**, 310–377.

SCHLICKEISER, R. 1989 Cosmic-ray transport and acceleration. I – Derivation of the kinetic equation and application to cosmic rays in static cold media. II – Cosmic rays in moving cold media with application to diffusive shock wave acceleration. *Astrophys. J.* **336**, 243–293.

SHALCHI, A. 2010*a* A unified particle diffusion theory for cross-field scattering: subdiffusion, recovery of diffusion, and diffusion in three-dimensional turbulence. *Astrophys. J.* **720**, L127–L130.

SHALCHI, A. 2010*b* Random walk of magnetic field lines in dynamical turbulence: a field line tracing method. I. Slab turbulence. *Phys. Plasmas* **17** (8), 082902.

SHALCHI, A. & KOLLY, A. 2013 Analytical description of field-line random walk in Goldreich–Sridhar turbulence. *Mon. Not. R. Astron. Soc.* **431**, 1923–1928.

SHALCHI, A. & KOURAKIS, I. 2007*a* Analytical description of stochastic field-line wandering in magnetic turbulence. *Phys. Plasmas* **14** (9), 092903–092903.

SHALCHI, A. & KOURAKIS, I. 2007*b* Random walk of magnetic field-lines for different values of the energy range spectral index. *Phys. Plasmas* **14** (11), 112901–112901.

SHEBALIN, J. V., MATTHAEUS, W. H. & MONTGOMERY, D. 1983 Anisotropy in mhd turbulence due to a mean magnetic field. *J. Plasma Phys.* **29**, 525–547.

SNODIN, A. P., RUFFOLO, D., OUGHTON, S., SERVIDIO, S. & MATTHAEUS, W. H. 2013 Magnetic field line random walk in models and simulations of reduced magnetohydrodynamic turbulence. *Astrophys. J.* **779**, 56.

SPATSCHEK, K. H. 2008 Aspects of stochastic transport in laboratory and astrophysical plasmas. *Plasma Phys. Control. Fusion* **50** (12), 124027.

SRIDHAR, S. & GOLDREICH, P. 1994 Toward a theory of interstellar turbulence. 1: weak Alfvenic turbulence. *Astrophys. J.* **432**, 612–621.

TENBARGE, J. M. & HOWES, G. G. 2012 Evidence of critical balance in kinetic Alfvén wave turbulence simulations. *Phys. Plasmas* **19** (5), 055901.

TENBARGE, J. M. & HOWES, G. G. 2013 Current sheets and collisionless damping in kinetic plasma turbulence. *Astrophys. J.* **771**, L27.

TENBARGE, J. M., HOWES, G. G. & DORLAND, W. 2013 Collisionless damping at electron scales in solar wind turbulence. *Astrophys. J.* **774**, 139.

TENBARGE, J. M., HOWES, G. G., DORLAND, W. & HAMMETT, G. W. 2014 An oscillating Langevin antenna for driving plasma turbulence simulations. *Comput. Phys. Commun.* **185**, 578–589.

WANG, E., NEVINS, W. M., CANDY, J., HATCH, D., TERRY, P. & GUTTENFELDER, W. 2011 Electron heat transport from stochastic fields in gyrokinetic simulationsa. *Phys. Plasmas* **18** (5), 056111.

ZIMBARDO, G., POMMOIS, P. & VELTRI, P. 2006 Superdiffusive and subdiffusive transport of energetic particles in solar wind anisotropic magnetic turbulence. *Astrophys. J.* **639**, L91–L94.

ZIMBARDO, G., VELTRI, P., BASILE, G. & PRINCIPATO, S. 1995 Anomalous diffusion and Lévy random walk of magnetic field lines in three dimensional turbulence. *Phys. Plasmas* **2**, 2653–2663.

ZIMBARDO, G., VELTRI, P. & POMMOIS, P. 2000 Anomalous, quasilinear, and percolative regimes for magnetic-field-line transport in axially symmetric turbulence. *Phys. Rev.* E **61**, 1940–1948.

ZWEBEN, S. J., MENYUK, C. R. & TAYLOR, R. J. 1979 Small-scale magnetic fluctuations inside the macrotor tokamak. *Phys. Rev. Lett.* **42**, 1270–1274.